Biomedicine and Chemical Sciences 1(3) (2022) 178-192

25-BCS-941-126

Contents lists available at:
https://journals.irapa.org/index.php/BCS/issue/view/12

Biomedicine and Chemical Sciences

Journal homepage: https://journals.irapa.org/index.php/BCS

Synthesis and Characterization of New Triazols Derivatives as C-Steel Reducing of Corrosion in Acidic Medium

May Jaleel Abed[a]*, Ahmed Ebrahim Hamzah[b], Kasim Kadhim Alasedi[c]

[a] *University of Al-Qadisiyah, College of Medicine, Medical Chemistry – Iraq*
[b,c] *Altoosi University College - Iraq*

ARTICLE INFO

Article history:
Received on: January 20, 2022
Revised on: May 10, 2022
Accepted on: March 02, 2022
Published on: July 01, 2022

Keywords:
$C_2H_3N_3$
Losing Weight
Reducing of Corrosion
Schiff Base
Acidic Solution

ABSTRACT

Six derivatives of novel triazoles were produced from some substituted benzoic acid with thiocarbazide via method of grinding. The produced Chemicals were described via ^{1}HNMR, IR, and ^{13}CNMR spectra examinations. Produced derivatives of $C_2H_3N_3$ were examined and assessed as reducing of corrosion in 0.5 M HCl for low-C steel utilizing procedure of losing weight. It was noticed that such chemicals had an encouraging act as reducer counter to mild steel corrosion of in solution being acidic. Reducing of maximum action was assessed at various concentrations and temperature of effector. Competence of corrosion reducer surpassed 96%. The exceptional action was due to inhibitor films adsorption development on surfacing steel. Reducing adsorption on surface of steel tracked Langmuir adsorption isotherm (LAI). The results were long-established by theoretical calculations of quantum chemistry.

1. Introduction

Steel might contacting solutions being acidic throughout pickling methods, metal cleaning, acidizing oil wells, etc. Such connection might be so serious and damaging to surfaces of metal. Surface of protecting metal counter to corrosion is an applied corrosion control ways in solutions being acidic (Jones, 1992). Organic Chemicals utilizing as reducing of corrosion metals in solutions as aqueous expected an excessive consideration in methods of industry and investigation. The mostly inhibitors active corrosion are such chemicals having heteroatoms i.e., N, S, O (Dubas & Schlenoff, 2001) and P, along rings being aromatic that are blocking the sites being active, declining the rate of corrosion. The Chemicals which are containing N and S displayed inhibition of excellent action in comparison to other Chemicals having only N or S (Mehta, et al., 2021).

Regarding organics of corrosion research, consideration is paid to the adsorption mechanism besides the relationship between structures of reducer and its properties of adsorption. It was noticed that the adsorption relies chiefly on the structural and usage molecule properties i.e., factors being steric, groups being functional, aromaticity, density of electrons on atoms being donor and donating e *p* orbital character (Chauhan et al., 2020). Likewise, reducers being efficient must have abundant p- e and unshared e pairs on reducers N or S atoms toward orbitals *d*- of Fe, and through e adsorption of chemical transference means might take place on surface of steel. Thus, the corrosion of steel might be inhibited via film being protective on the surface of steel (Lahbib et al., 2020). In the suitable compound selection for reducing of corrosion, the compound properties (electronic and geometric) effect the compound ability for surface covering of metal as well as compound capacity for reacting with surface of metal; thus, just surface binding to the metal. In probing for appropriate reducers being organic of corrosion, many investigators have stated some derivatives of $C_2H_3N_3$role as inhibitors of corrosion on various surfaces of metals and in various surroundings (Onyeachu & Solomon 2020).

***Corresponding author:** May Jaleel Abed, University of Al-Qadisiyah, College of Medicine, Medical Chemistry – Iraq

E-mail: **may.abed@qu.edu.iq**

How to cite:

Abed, M. J., Hamzah, A. E., & Alasedi, K. K. (2022). Synthesis and Characterization of New Triazols Derivatives as C-Steel Reducing of Corrosion in Acidic Medium. Biomedicine and Chemical Sciences, 1(3), 178–192.

DOI: **https://doi.org/10.48112/bcs.v1i3.126**

Thus, methods as quantum chemical joint with methods of experimental were employed to approve derivatives of $C_2H_3N_3$ potential being reducing of corrosion. In the current work, 6 derivatives of $C_2H_3N_3$were produced and confirmed as steel corrosion reducers in solution being acidic (Chauhan et al., 2020).

2. Materials and Methods

2.1. Synthesis of Corrosion Reducing Derivatives

Process of reaction and yield ion was performed in a (200 ml) flask round- bottomed enclosed in a H_2O bath. For keeping uniform distribution of temperature, magnetic stirrer was utilized in flask that was furnished with condenser as reflux where temperature was organized utilizing heater of hot plate.

2-(4-Amino-5-mercapto-4H-1,2,4- triazole-3-yl*)benzene-,3-ol* (A_1) was produced via 3-hydroxy benzoic acid (0.01 mol) fusion and thiocarbazide (0.015 mol) in test tube dipped in bath of oil for controlling temperature. Hotplate was utilized as heating source. Temperature of reaction was 145 °C. The yield obtained on cooling was preserved in (200 ml) flask round-bottomed with solution of $NaHCO_3$ at 78 °C for neutralizing carboxylic acid that unreacted. Bath of H_2O was utilized for controlling temperature. Then, it was washed with H_2O and collected via filtration. Similar apparatus and tools were utilized in yield ion other reducers. Moreover, temperatures of reaction for neutralization and fusion process were similar (145 and 78 °C, respectively). *4-Amino-5-(pyridine-2-ol)-4H-1,2,4-* $C_2H_3N_3$ *-3-thi- aol* (A_2) was produced via p- OH $C_5H_4N(CO_2H)$ (0.02 mol, 2.23 g) fusion and CH_6N_4S (0.03 mol, 3.8 g). The obtained yield on cooling was cured with solution of $NaHCO_3$ for neutralizing carboxylic acid derivative that unreacted. Then, it was washed with H_2O and via filtration was collected.

4-Amino-5-(3-(((Z)benzylidene) amino)-4- amino) phenyl)-4H-1,2,4- $C_2H_3N_3$ *-3-thiaol* (A_3) was produced via benzylidene) $C_6H_5CO_2H$ (0.002 mol, 1.6 g) fusion and thio-carbohydrazide (0.015 mol, 0.62 g). On cooling, the obtained yield was cured with solution of $NaHCO_3$ for neutralizing carboxylic acid that unreacted. Then, with H_2O was washed and via filtration was collected. *5,5 '-(((1,4-Phenylenebis(methanylylidene)) bis(azanylylidene))bis(4,1-phenylene-2-Ol))bis(4-amino-1,2,4-* $C_2H_3N_3$ *-3-thiol)* (A_4) *and 4-amino -5-(4-((4-(4-amino- 5-mercapto-4H-1,2,4-triazol-3-yl)benzylidene)amino) phenyl-2Ol)-4H-1,2,4-* $C_2H_3N_3$ *-3-thiaol* (A_5) were produced via Chemicals fusion replaced by (0.002 mol) $C_6H_5CO_2H$-3-OH and (0.012 mol) CH_6N_4S. On cooling, the obtained yield was cured with solution of $NaHCO_3$ for neutralizing carboxylic acid that unreacted. Then, with H_2O was washed and via filtration was collected. *4-((4-(4-Amino-5-mercapto-4H-1, 2, 4-* triazole *-3-yl) benzylidene) amino)-1, 5-dimethyl-2-pheny-4 nitro-(4-nitro)-1, 2-dihydro- 3H-pyrazol-3-one* (A_6) had been produced via [A_5] (1.2 g, 0.004 mol) fusion and CH_6N_4S (0.62 g, 0.006 mol). On cooling, the gotten yield was cured via solution of $NaHCO_3$ for neutralizing carboxylic acid that unreacted. Then, with H_2O was washed and via filtration was collected.

For the foregoing, the reaction achievement along compound purity was tested via (TLC, hexane: ethyl acetate as mobile phase 1:2). The yield was crystallized again from suitable solvent for giving compound being as title (Li et al. 2020). Figure 1 illustrates the corrosion reducing synthesis system (A1–A6).

2.2. Calculations of Chemical Quantum

Calculations being theoretical of chemical quantum widely have been engaged for simulates the process of reducing of corrosion. The parameters of structure, occupied highest orbital of molecule, unoccupied lowest orbital of molecule, moment of dipole (μ), and electron transferred fraction were measured and improved via software of *ChemoOffice* version 14.

2.3. Analysis NMR and Fourier IR transform (FTIR)

FTIR spectra were proved in spectrophotometer that achieved from 400 to 4000 cm^{-1}, utilizing technique of NMR, KBr disk, ^{13}CNMR and ^{1}H- spectroscopy were utilized in reducing of corrosion diagnosis and analysis process.

2.4. Measurements of Losing Weight

Low-C steel exam sample has chemical constituents as following (wt%): 0.000 Ti, 0.0067 S, 0.033 Si, 0.0056 P, 0.0476 Cu, 0.057 Al, 0.1 C, 0.335 Mn, 0.0201 Cr, 0.001 Co, and Fe as balance. Rectangular samples test are of dimensions 3 × 1 × 0.1 cm revealing an estimated 6.8 cm^2 surface area. Before every measurement, sample of steel was scraped with papers of emery grade (400–1000), ultrasonically washed with D.W, alcohol and acetone, at air being dry was dried, and then reserved in over silica bed gel desiccators till utilize. Every sample dimensions by a vernier were measured to the 2nd millimeter decimal and weighted precisely to 4th g decimal. Electrolyte testing of solution being aqueous 0.5 M HCl was arranged via dilution Grade Analar 37% HCl with H_2O ultra-pure. Samples of metal were immersed entirely in 500 ml of reducers and unreducers.

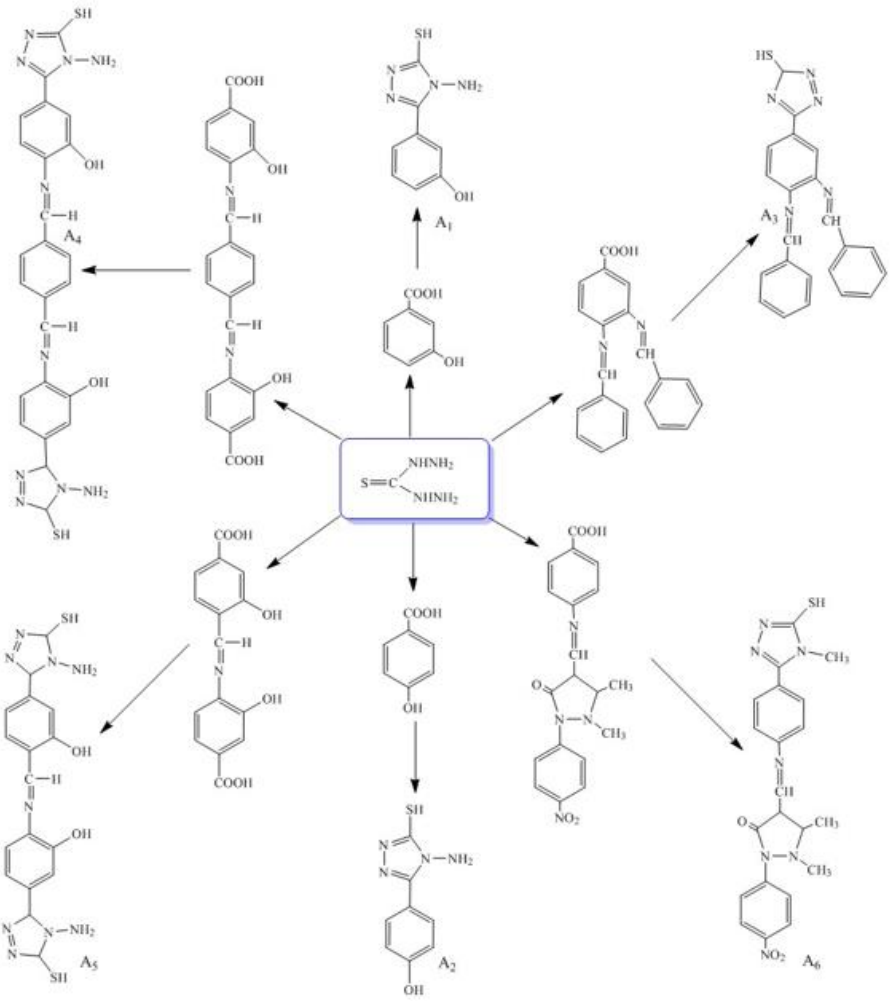

Fig. 1. Corrosion reducers (A_1–A_6) synthesis system

0.5 M solution of HCl confined in flask as conical. Bath of H_2O was utilized for controlling temperature. They were subjected for 3 hs wanted concentration and temperature of inhibitor. After that, metal samples were cleaned, washing by tap running H_2O then through D.W, drying with tissue being clean, and after that submerged in alcohol and acetone and again dried. Losses of weight in g/m^2/day (gmd) were firmed in reducer existence and absence. At starting, whole reducers were examined at concentration of inhibitor 0.001 M and 30 °C for selecting the top one. higher efficiency of prepared derivatives then was assesed at various temperatures (20, 30, 40, and 50 °C) and concentration of reducer of 1×10^{-3}, 2×10^{-3}, 3×10^{-3}, and 4×10^{-3} M. Measurements as whole were done 3 times to obtain reproducibility being satisfactory.

3. Results and Discussion

3.1. Reducing of Corrosion Identifies

FTIR spectra and NMR, ^{13}CNMR and ^{1}HNMR spectroscopy were utilized in the reducing of corrosion diagnosis and analysis process. Figures 2-6 illustrate inhibitors NMR and FTIR spectrum. The groups being active and specifications were determined. Detected values for A1 show absorbance peak for amine group at (3356), hydroxy group (3568), stretching peak for hydrogen amine in (3283), C=N_{str} in triazole ring (1654), C-S (1241), C–H_{str} in aromatic ring in (3173), C=C_{str} in aromatic ring (1566, 1497). ^{1}HNMR spectrum of compound seems to have data as follow: (Singlet signal in 8.4 for SH), (Singlet signal in 12.5 for OH), (Singlet signal in 5.2 for hydrogen of amine group). A_2 shows peak in (3432–3323) cm^{-1} for amine group, stretching peak in (3178) for hydrogen amine , stretching peak for aromatic hydrogen (3087), stretching peak in (1636) for C=N group. ^{1}HNMR spectrum (400 MHz, d6-DMSO, ppm) of (S_6) compound seems to have data as follow: (Singlet signal in 5.3 for hydrogen of amine group), Singlet signal 8.7 in for hydrogen of SH group, Signal in 6.02–7.1 ppm for hydrogen of aromatic ring. Specifications as follow were noticed for A_3: stretching peak in (3071)cm-1 for hydrogen amine , stretching peak in (3001)cm^{-1} for aromatic hydrogen, stretching peak in (2942)cm^{-1} for aliphatic hydrogen, stretching peak in (1617)cm^{-1} for C=N group, stretching peak in (1445)cm^{-1} for C=C group, (1241)cm^{-1} for C=S group NH_2 peak in (3480–3422) cm^{-1}.

^{1}HNMR spectrum (400 MHz, d6-DMSO, ppm) of (S14) seems to have information as follow 8.3 (S, 2H, N=CH),: δH = 10.5 (S, 1H, SH), 5.8 (S, 2H, NH2). For A_4 stretching peak in (3483–3418) cm^{-1} for amine group , stretching peak in (3134) cm^{-1} for hydrogen of amine group , stretching peak in (3011) cm^{-1} for aromatic hydrogen , stretching peak in(1614) cm^{-1} for cyano group, stretching peak in (1323) cm^{-1} for C=S group, stretching peak in (1505–1414) cm^{-1} for C=C group. ^{1}HNMR spectrums 7.9–8.2 (7H, Aromatic H), of (400 MHz, d6-DMSO, ppm) of A_4compound seems to have data as follow: δH = 8.7 (S, 2H, N=CH), 10.7 (S, 1H, SH), 7.1–8.3 (8H, Aromatic H) 5.5 (S, 2H, NH2). ^{13}CNMR (400 MHz, d6-DMSO, ppm): 143, 126 (Ar–CH) δC = 164 (CH=N) 135 (N–C–N), 149. Nevertheless, A_5 specifications are: C=Cstr (1504–1434), N–Hstr (3128), aromatic C–Hstr (2995), NH2 (3276–3166), C=Nstr(1588), C=S (1237), yield: 70%. ^{1}HNMR spectrum (400 MHz, d6-DMSO, ppm) of (S17) compound seems to have data as follow: 8.7 (S, 2H, N=CH), 7.6–8.2 (4H, Aromatic H) 5.5 (S, 2H, NH2), δH = 10.9 (S, 1H, SH) . ^{13}CNMR (400 MHz, d6-DMSO, ppm):

δC = 167 (CH=N), 131 (N–C–N), 149, 142, 138, 129, 128, 125 (Ar–CH). A_6 specifications are as follow: stretching peak in (3185) cm^{-1} for hydrogen of amine group, stretching peak in (2931) cm^{-1} for aromatic hydrogen , NH_2 stretching peak in (3374–3287) $cm^{-1}$for amine group , stretching peak in (1596), C=S (1309) cm^{-1} for cyano group, yield: 64%. ^{1}HNMR spectrum (400 MHz, d6-DMSO, ppm) of A_6 compound seems to have data as follow: δH = 9.6 (S, 1H, SH), 8.3 (S, 2H, N=CH), 7.3–7.9 (4H, Aromatic H), 5.5 (S, 2H, NH2), 2.1 (S, 6H, 2CH3). Table 1 illustrates physical inhibitor characters.

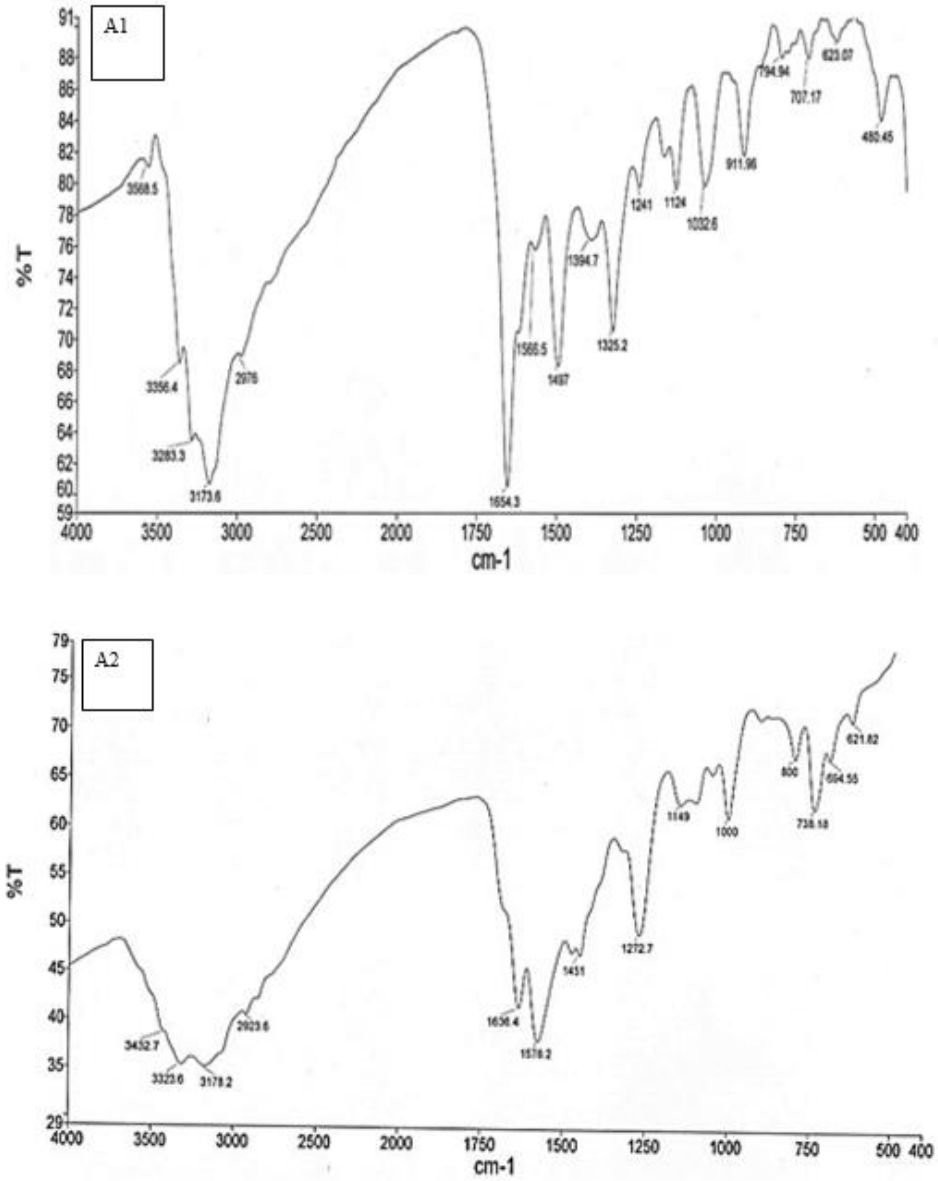

Fig. 2. FTIR spectrum of reducers(A_1,A_2)

3.2. Measurements of Weight Losing

Table 2 reviews losing weight of low-C steel alloy corrosion technique results in 0.5 M HCl solution of at 0.001 M concentration and 30 °C of inhibitor. Rate of corrosions values was determined utilizing the equation as follow (Godínez, et al., 2020):

$$CR = \frac{\text{weight lossing(g)}}{\text{Area(m}^2\text{)X time(day)}}$$

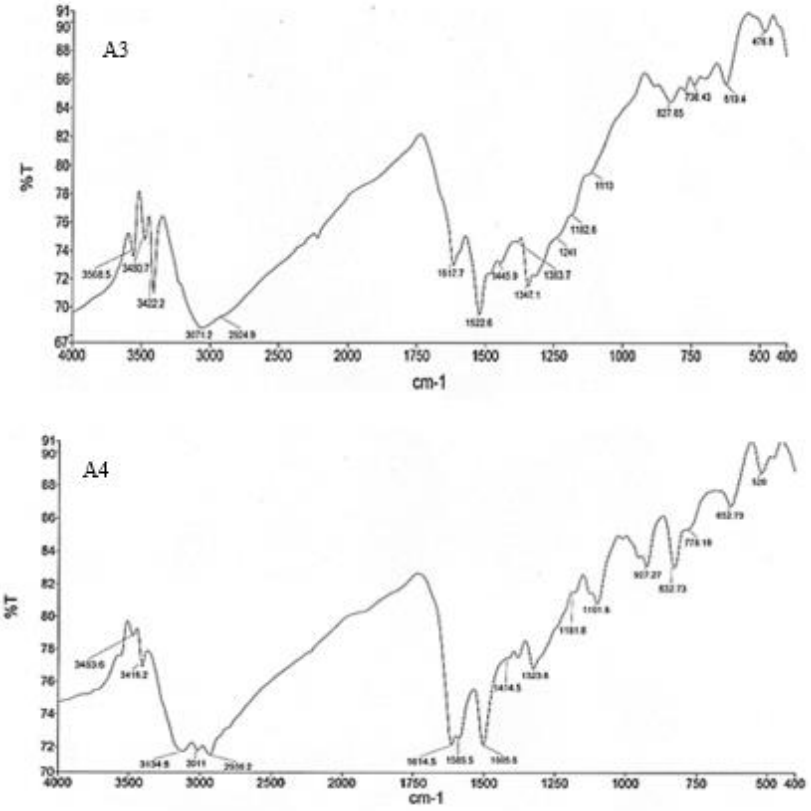

Fig. 3. FTIR spectrum of reducers(A_3,A_4)

Through rate of corrosion, reducing % efficiency of experiments loss weight (%IE) was measured utilizing eq. as follow (Burns, 1936):

$$\%IE = \frac{CR_{unreduced} - CR_{reduced}}{CR} X\ 100$$

Since $CR_{unreduced}$ and $CR_{reduced}$ are the rates of corrosion at inhibitors absence and presence, respectively. Table 2 illustrates the efficiency of reducer ranging from 72.89 to 81.08%. A4 illustrates action as the higher. For having A4 behavior clear vision, temperature and reducing concentration effects were considered. Table 3 illustrates the results. Rate of corrosion augmented with temperature upsurge and decline of concentration of reducer, while efficiency of prepared reducer augmented with the elevation temperature and concentration of inhibitor (Godínez, et al., 2020).

There were inspected recently produced S having Schiff base compound (4-((thiophene-2-ylmethylene) amino) benzamide). Reducing action on steel mild in1.0 M HCl solution was considered. Observations illustrated the highest efficiency of inhibitor of 96.8% (Joy, et al., 2013). Studies for the influence of recently produced thiazole hydrazones on the mild corrosion steel in HCl 0.5 M. inhibitors adsorption tracked isotherm of Langmuir and inhibitors addition decreased simultaneously rate of corroion.

Messali, et al., (2018) reviewed the influence of behavior of adsorption and inhibition of 4-((2,3- dichlorobenzylidene).

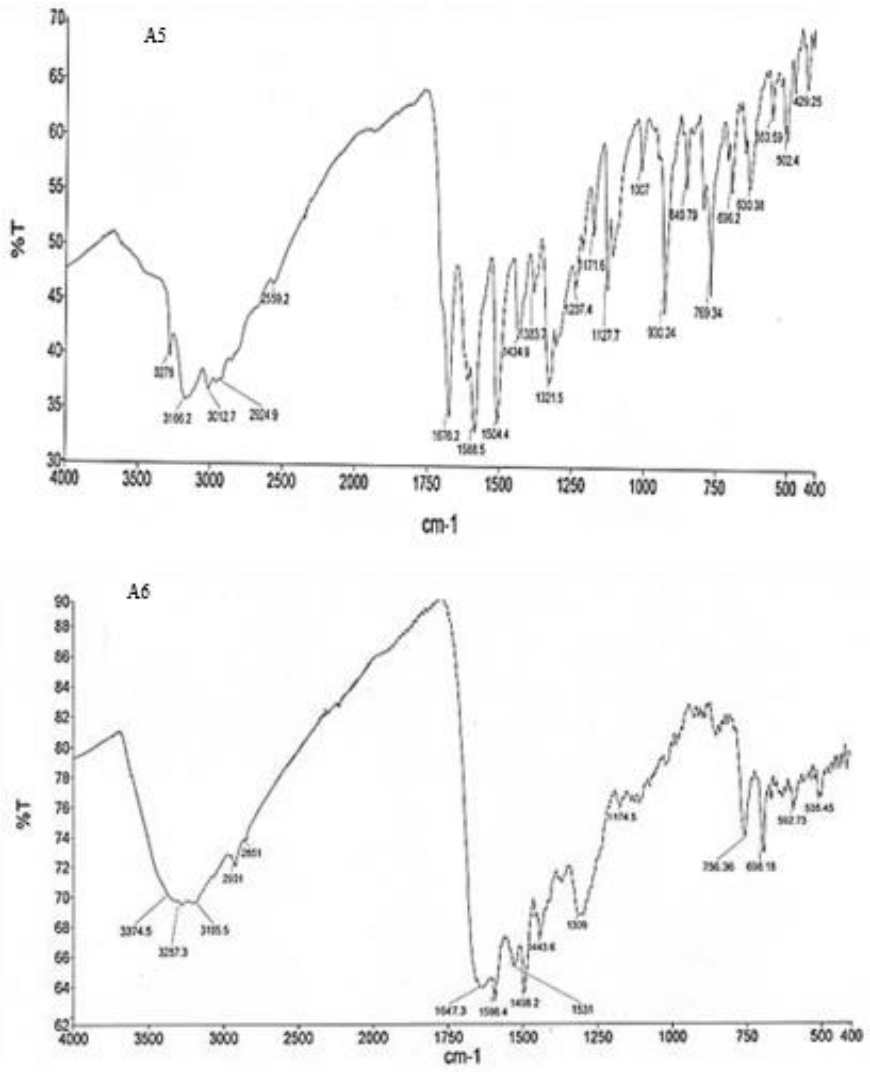

Fig. 4. FTIR spectrum of reducers(A_5,A_6)

3.3. Concentration of Inhibitor Influence and Invistigations of Adsorping

As illustrated in Table 3, at temperature being explicit, corrosion steel rate declines by elevation in concentration of A_4. Reducers efficiency values elevate with A_4 concentration elevation and reach 96.02% as maximum value at higher concentration of inhibitor and temperature level. Such elevation in reducing act of temperature is seemingly because of an elevation in inhibitor chemisorption. Vital stage in reducing action behavior in medium being acidic is frequently agreed on the surface of metal adsorption. Such including the postulation that the reactions of corrosion are banned from happening over surface of metal active sites or the area sheltered via adsorbed molecules of reducer , while these reactions of corrosion generally occurred on the free active sites of reducer (Zhu, et al., 2021). The data of coverage of surface (θ = %IE/100) are so valued in conversing features of adsorption. Covered surface is associated with inhibitor concentration at temperature being constant through recognized relationships of isotherm of adsorption, which are determined at condition at equilibrium. The θ dependence on A_4 concentration was graphically tested via fitting it to LAI which adopts surface of metal has a fixed adsorption sites number and every site only takes one molecule being adsorbed. Figure 8 illustrates plots as linear for C/θ against C of average R2 = 0.99 coefficient of correlation, proposing adsorption is following the LAI (Dheeraj, et al 2020):

$$\frac{C}{\theta} = \frac{1}{K} + C \quad \ldots\ldots\ldots\ldots \qquad (3)$$

$$K = \frac{1}{55.5} exp \frac{\Delta Gads}{RT} \ldots\ldots \qquad (4)$$

Since C is the reducer concentration and K is adsorption constant of equilibrium, demonstrating the adsorption degree; which means, the upper the K value

identifies that molecules of A_4 is adsorbed strongly on the surface of which means that every molecule of inhibitor reside in 1 site active on the surface of metal. The free adsorption standard energy (ΔGads) was measured as above utilizing equ as follows (Wang, et al., 2015): metal. T Langmuir adsorption slops of lines are nearby unity since 55.5 is H_2O concentration in solution stated in M, R is the constant of gas, and T is the temperature as absolute. Table 4 illustrates the parameters of adsorption (Younis, et al., 2020).

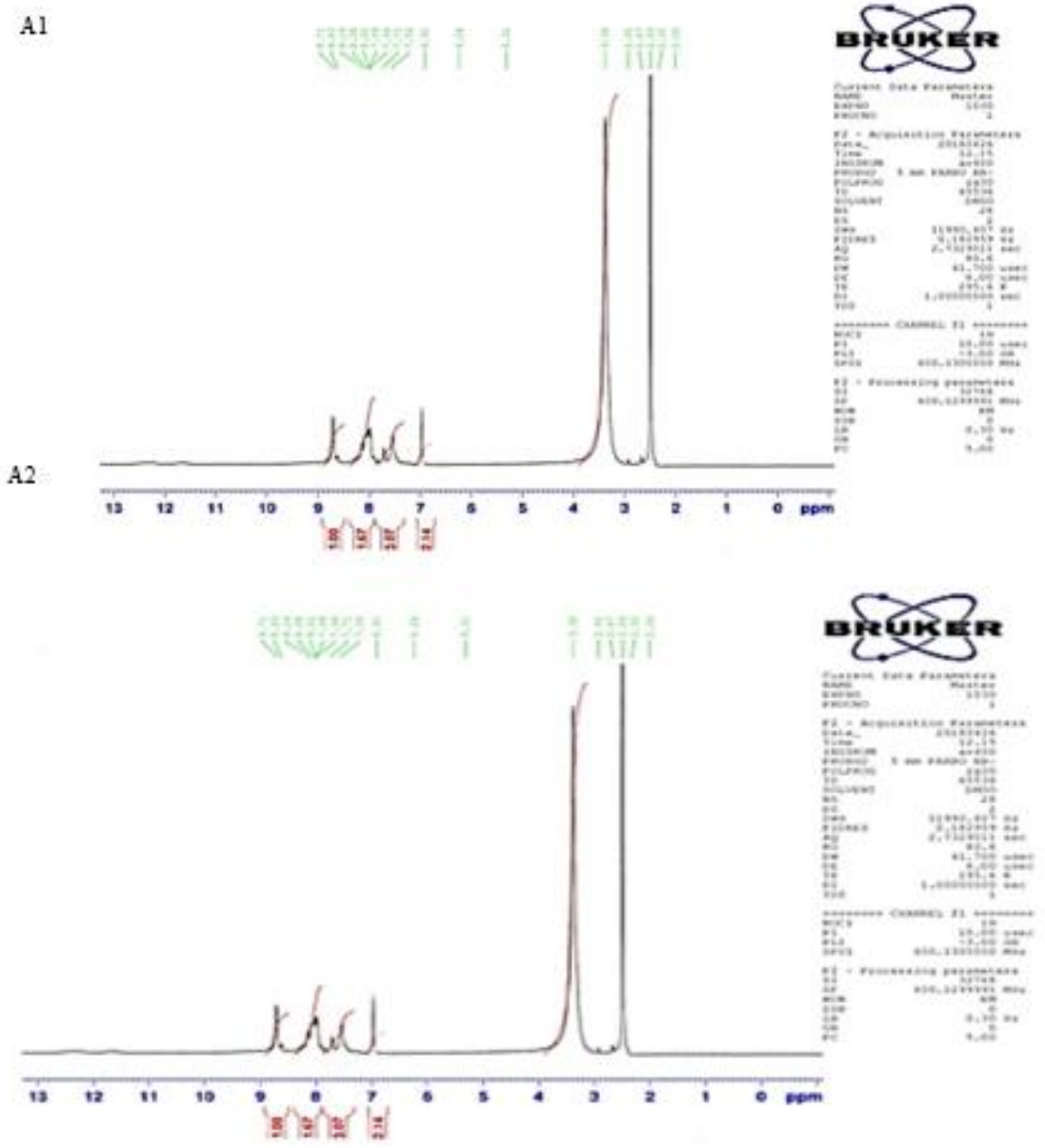

Fig. 5. ^{1}HNMR spectrum of reducers(A_1,A_2)

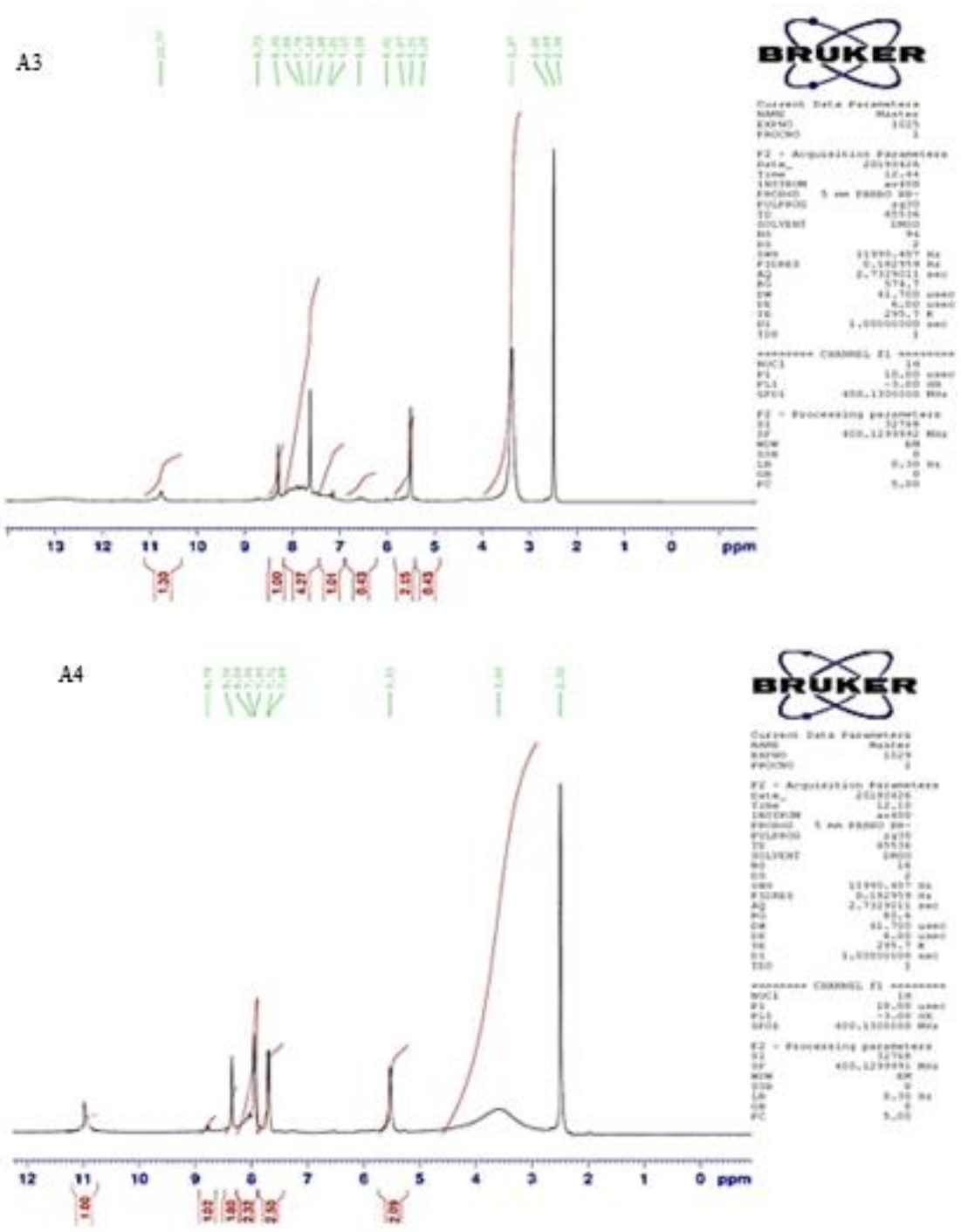

Fig. 6. ^{1}HNMR spectrum of reducers(A_3 and A_4)

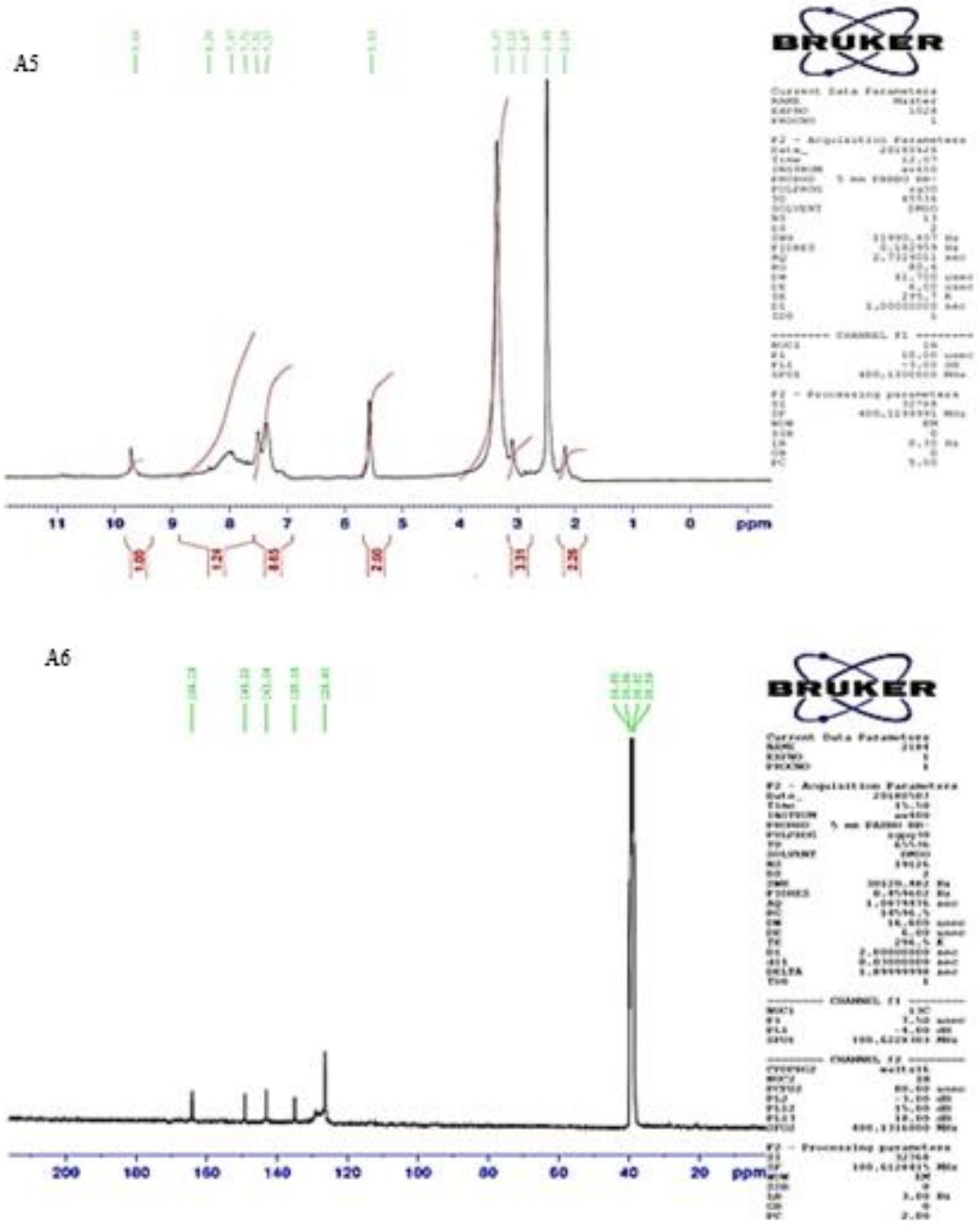

Fig. 7. ^{1}HNMR spectrum of reducers (A_5 and A_6)

The standard average free energy adsorption value was− 34.85 kJ/mol. The negative $\Delta G_{ads}°$ value guarantees the adsorption spontaneous course and layer adsorbed constancy on metal the surface. Frequently, the $\Delta G_{ads}°$value up to − 20 kJ/mol is steady of electrostatic interface between molecules being charged and the metal being charged (adsorption being physical), whereas these nearby − 40 kJ/mol or upper are related to chemically adsorption being results of haring or electron transfer to the surface from molecules of metal forming a coordinate bond type (Yang, et al., 2020).

Nevertheless, other workers proposed that the standard adsorption range of chemical adsorption methods free energy for reducers in media being aqueous deceits between − 21 and − 42 kJ/ mol (Feng, et al 2020). Thus, regarding current work the adsorption heat values was regarded within the chemical adsorption range. Table 4 illustrates a partial surge in ΔG_{ads} value as absolute with increasing temperatures, demonstrating that adsorpting was somehow satisfactory with elevating temperature and adsorbed A_4 based on mechanism being chemical.

Table 1
Synthesis Chemicals Physical characters

reducer	m.p. (°C)	Color	Mol. Formula	Res. solvent	% Yield
A1	231–233	Deep brown	$C_8H_7N_4O_1S$	Ethanol/water	67
A2	193–195	Yellow	$C_7H_5N_3O_2S$	Ethanol/water	70
A3	>300	Deep brown	C22H16N6S	Ethanol/water	78
A4	263–265	Green	C24H22N10O_2S2	Ethanol/water	76
A5	287–289	Yellow	C17H17N9 O_2S2	Ethanol/water	70
A6	207–209	Orange	C20H19N8O_3S	Ethanol/wat	64

Table 2
Low-C steel alloy corrosion rate and synthesis Chemicals corrosion inhibitor efficiency in solution 0.5 M HCl at 30 °C and inhibitor 0.001 M concentration

Reducer	Form.	rate of corrosion (g/m2 day)		
A_1	$C_8H_7N_4O_1S$	17.2	75.8	0.18
A_2	$C_7H_5N_3O_2S$	18.6	77	0.2
A_3	$C_{22}H_{16}N_6S$	21.6	73.2	0.23
A_4	$C_{24}H_{22}N_{10}O_2S_2$	15.2	81.1	0.16
A_5	$C_{17}H_{17}N_9$ O_2S_2	35.2	78.2	0.37
A_6	$C_{20}H_{19}N_8O_3S$	21.8	72.9	0.23

3.4. Temperature Influence and Activation Revisions

Table 5 illustrated at temperature being explicit steel rate of corrosion declines with A_4 elevation in concentration. A_4 action as kinetics can be recognized via comparing parameters of activation in the inhibitor absence and presence. (ΔH_a), (ΔS_a) and energy of Activation (E_a), 0.5 M HCl for reducing corrosion steel at several concentrations and temperatures of acid were determined from plot of Arrhenius-type (Eq. 5) and state theory of transition (Eq. 6) (Georgopoulou & Clemens, 2020) efficiency of inhibitor (%).

Table 3
Corrosion rate of low-carbon steel alloy and inhibitor efficiency of synthesis A4 in 0.5 M hydrochloric acid solution at different conditions

Test #	Concentration of reducer (M)	Temp. (°C)	Rate of corrosion (g/m2 day)	Efficiency of reducing (%)	Standard deviation (SD)
1	0	20	75.39	–	1.938
2	0	30	80.52	–	2.138
3	0	40	154.79	–	2.032
4	0	50	420.05	–	3.371
5	1 × 10−3	20	10.29	86.35	0.401
6	2 × 10−3		7.78	89.67	0.303
7	3 × 10−3		7.35	90.24	0.286
8	4 × 10−3		6.14	91.84	0.239
9	1 × 10−3	30	15.33	80.95	0.597
10	2 × 10−3		15.23	81.08	0.593
11	3 × 10−3		13.43	83.31	0.523
12	4 × 10−3		10.78	86.61	0.421
16	1 × 10−3	40	21.17	86.32	0.825
14	2 × 10−3		21.04	86.4	0.821
15	3 × 10−3		20.97	86.45	0.817
16	4 × 10−3		16.39	89.4	0.639
17	1 × 10−3	50	27.89	93.35	1.087
18	2 × 10−3		17.89	95.74	0.697
19	3 × 10−3		16.81	95.99	0.655
20	4 × 10−3		16.68	96.02	0.651

$$CR = A \exp\left(-\frac{Ea}{RT}\right)$$

Table 4
A4 Parameters of adsorption at various temperatures

T (°C)	K (M−1)	Slop	R^2	ΔGads (kJ/mol)
20	10471.2	1.07	0.99	− 32.33
30	11005.4	1.13	0.99	− 33.56
40	12706.5	1.11	0.99	− 35.04
50	30303.3	1.03	0.99	− 38.49
Average value	16121.6	1.09	0.99	− 34.85

Table 5
Parameters of activation for corrosion of steel reaction in inhibited and uninhibited0.5 M HCl

C (M)	A (gmd)	E_a (kJ/mol)	ΔH_a (kJ/mol)	ΔS_a (J/mol K)
0	6.5 × 109	45.18	42.63	− 65.02
1 × 10−3	4.7 × 105	26.12	23.56	− 144.33
2 × 10−3	1.1 × 105	22.61	20.05	− 157.23
3 × 10−3	1.3 × 105	23.44	20.88	− 155.06
4 × 10−3	4.7 × 105	27.15	24.58	− 144.41

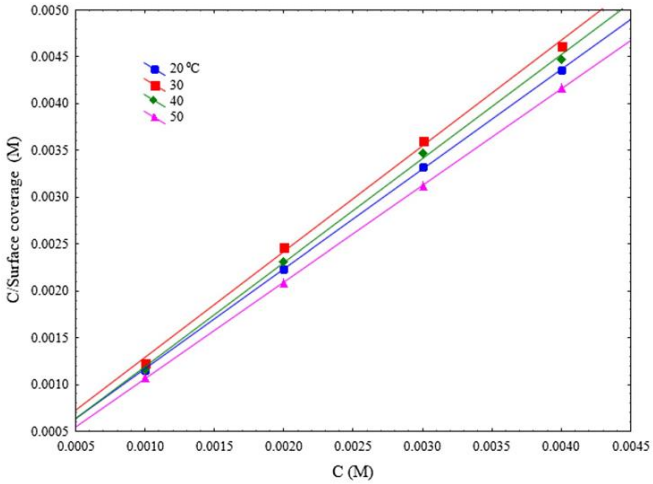

Fig. 8. A_4 LAI on the surface of steel in solution 0.5 M HCl at various temp

Liner straight ln(CR/T) lines against slopes of 1/T of ΔHa/R and intercept might be utilized for determining ΔSa. Table 5 displays parameters of corrosion activation of steel

acidic reaction solution at various circumstances. It is obviously exposed energy of activation and enthalpy differs in a alike way. Enthalpy and activation energies for acid that uninhibited were greater than the inhibited one. Enthalpy and activation energies decline values looks to be undependable. Nevertheless, such might be because of the metal coverage surface surge via molecules of reducer at greater temperatures and proposed chemisorbed layer rate formation might be superior to its dissolution rate at greater temperatures (Gao, et al., 2018).

Other workers stated few materials as anticorrosion in solutions being acidic modify the corrosion reaction kinetics via suggesting paths of alternative reaction with lower energies of activation. In addition, Table 5 displays that whole factor frequency values are less compared to uninhibited one that is advantegeous for corrosion steel rate reducing. In addition, it is famous that the elevation in A elevates the corrosion of steel rate (Zhang, et al., 2020).

Moreover, in whole cases Ea values are greater than ΔHa by a value which is almost = RT, that approve the equation 6.

$$CR=\frac{RT}{Nh}\exp\left(\frac{\Delta Sa}{R}\right)\exp\left(-\frac{\Delta Ha}{RT}\right)\text{.....(6)}$$

Where CR is the corrosion rate, A is constant of Arrhenius, R is universal gas constant, h is constant of Plank , and N is number of Avogadro. Figure 9 illustrated in, ln (CR) plot as opposed to 1/T offers lines being straight of ΔEa/R slopes along intercept might be utilized for assessing A, whereas Figure 10 illustrates a the equation as follow (Lei, et al., 2021):

$$Ea-\Delta Ha=RT\text{.....(7)}$$

The ΔSa negative value for reducer presence and absence specifies that complex activated in the determining step rate represents relationship rather than step of detachment that specifies a decline in disturbance occur throughout the transition course from reactant to the complex activated (Xiong, et al 2021).

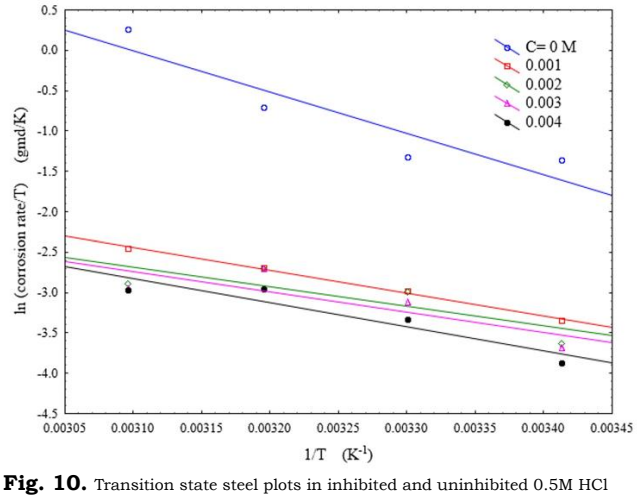

Fig. 10. Transition state steel plots in inhibited and uninhibited 0.5M HCl

3.5. Chemical as Quantum and Calculations being Theoretical

Quantum chemical calculations was utilized widely for investigation reaction of inhibition process mechanism (Arzaee, et al., 2021). In addition, it is proved to be a so vital tool for evaluating mechanism of corrosion control and obtaining view insight to the inhibitors reducing mechanism. Via utilizing quantum chemical calculations, the parameters of structure, i.e., HOMO (maximum molecular orbital occupied), LUMO (lowermost molecular unoccupied orbital).

Dipole moment (μ), and e transferred fraction (ΔN), were measured. Figures 11 and 12 display the structures being optimized, LUMO and HOMO production reducers structure. The measured properties of chemical quantum are shortened in Table 6. As displays in Figures 11 and 12, distributions of LUMO and HOMO as production inhibitors were mostly focused over atoms of S and N E_{HOMO} and E_{LUMO} described the e-receiving and e-donating synthesis inhibitors competence. Generally, E_{LUMO} being low suggests that reducers have a tendency to to accept e, whereas a high E_{HOMO} suggests to a tendency to e- donating.

(Δ*E*) energy gap postulates the chemical inhibitors stability, and a lower gap of energy value classically causes greater metal adsorpting surface, causing bigger efficiencies of reduce corrosion. The energy gap order was $A_4 > A_5 > A_2 > A_1 > A_3 > A_6$, that is in covenant with the inhibition order efficiency obtained from other studies.

In addition, e transferred number (Δ*N*) was measured based on Eq. (8).

$$\Delta N=\left(\frac{X\,Fe-X\,inh}{2(\eta\,Fe-\eta\,inh}\right) \quad \text{.....(8)}$$

Since X_{inh} and X_{Fe} represent molecules reducers and the absolute Fe electronegativity, respectively; η_{Fe} and η_{inh} signify the absolute Fe hardness and the inhibitor molecule, respectively. Quantities as such are linked to e affinity (*A*) and potential of ionization (*I*) which associated in sequence to E_{LUMO} and E_{HOMO}:

$$X=\frac{1+A}{2}=\frac{-(E\,Homo-E\,Lumo)}{2}\text{.....(9)}$$

$$\eta=\frac{1-A}{2}=\frac{-(E\,Homo-E\,Lumo)}{2}$$

X and *η* values were well-thought-out utilizing the *I and A values* of gotten from quantum calculation chemical. The X_{Fe} theoretical value is 7 based on's electronegativity scale of Pearson and η_{Fe} is 0 eV/mol, respectively (Gan, et al., 2019).

The e transferred fraction from reducer to the surface of steel (ΔN) was measured as shown in Table 6. Based on Lukovits, when $\Delta N < 3.6$, the efficiency of reducing elevated with elevating capacity of e-donating at the surface of steel. In the current work, producing inhibitors were the donating e and metal surface being acceptor. Such results aid the affirmation that inhibitors adsorbing on the surface steel can take place on the interactions foundations of acceptor–donor between the compound Λ e and the vacant surface of steel *d*-orbitals (Xing, et al., 2021). Also, dipole moment (*μ*) is a noteworthy aspect and there is covenant absence on connection between *μ* and action of reducing. Some workers stated that value as low *μ* will errand inhibitor amassing on surface of metal and elevating the inhibitor action (Li, et al 2021).

Whereas other workers proposed that a high dipole moment value related to the dipole–dipole inhibitor interface and metal surface might encourage the adsorbing on the

surface of metal and elevating effectiveness (Tom, et al., 2020).

At the current study, the μ value for A_4 was the upper one among all verified reducers that approve with the 2nd view. Such may be because of the true that O, S, N, and some C atoms of great masses of charges. The highest electron density regions are frequently the sites where electrophiles can confer (Blachowicz & Ehrmann, 2020). Thus, such atoms are centers being active that have the great capability to link to the surface of steel. The relative A_4 greater efficiency may be because of higher C atoms number in comparison to other inhibitors (Khaled, 2008).

(83) Utilized technique of simulation molecularly for optimizing derivatives of $C_2H_3N_3$ structure as inhibitor of corrosion for Fe. Data theoretically or experimentaly displayed that C2H4N4 of greatest inhibitor among C2H4N4, $C_2H_3N_3$, and benzo $C_2H_3N_3$. Also, Babić-Samardžija & Hackerman (Babić-Samardžija & Hackerman, 2006) implemented molecular model for getting perceptions into structural and polypyrazolylborates eic properties, dihydrobis (1-pyrazolyl) borate, and hydrotris(1-pyrazolyl) borate in respect to behavior of reducing efficiencies and adsorption. Based on electrochemical findings measurements, polypyra- zolylborates relatively were effectual inhibitors versus acidic Fe corrosion (Lebrini, et al, 2006) showed 2,5-bis(4-pyridyl)-1,3,4-thiadiazole (4-PTH) influence and few of their derivatives on the steel mild corrosion in medium being acidic via technique of quantum chemical. Energies of LUMO and HOMO electrons and dipole moments were determined. Such parameters in a model were interrelated with coefficient correlation greater than 0.93 which specified excellent correlation between the inhibition of corrosion and reducing structure (Liu, et al., 2019). Other studies showed the inhibition reliance efficiencies of 3three Chemicals (heterocyclic) utilizing the method of chemical quantum. Parameters, i.e., the LUMO and HOMO energies, gap of energy, dipole moments, net atomic charges, interaction and total energies, were measured. A worthy covenant was detected between experimentally and theoretically information.

Table 6
Calculated prepared inhibitors chemical quantum parameters

Chemicals	EHOMO (eV)	ELUMO (eV)	ΔE (eV)	ΔN	μ (Debye)
A_1	− 7.828	− 5.236	2.592	0.19	5.11
A_2	− 7.690	− 5.716	1.974	0.15	6.64
A_3	− 7.840	− 1.318	6.522	0.37	4.35
A_4	− 6.981	− 5.711	1.271	0.52	11.2
A_5	− 5.551	− 2.728	2.823	1.01	6.92
A_6	− 7.675	− 0.606	7.069	0.41	3.17

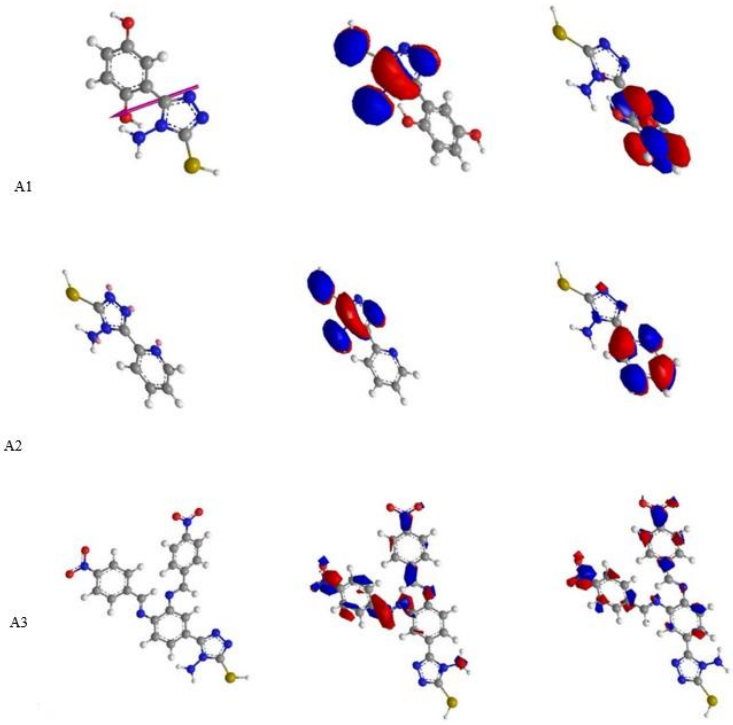

Fig. 11. Structure of A1, A2 and A3

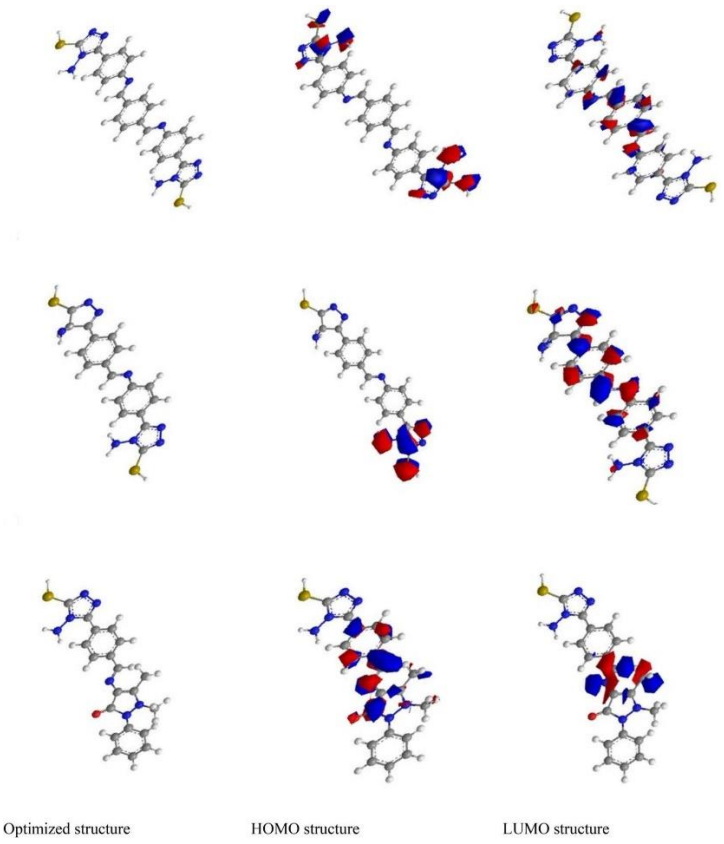

Fig. 12. Structure of A4, A5 and A6

4. Conclusions

The following might be summarized as conclusions;

The 6 reducers were formed and verified effectively in acidic solution as steel reducing corrosion.

1. Results of experiment reveal that the inhibition efficiency order was $A_4 > A_5 > A_2 > A_1 > A_3 > A_6$.
2. A_4 addition to solution of 0.5 M HCl at various concentrations and temperatures of reducers minimizes mild corrosion steel with competence of inhibitor beyond 96.02%.
3. Efficiency of A4 reducer amplified upsurge in concentration of reducer. The high inhibitor competence inhibition was because of layer formation on the steel surface.
4. Adsorption tracks LAI with high negative adsorption heat value indicate that the chemical layer was formed on metal surface.
5. Experiments were agreed and verified with theoretical calculations of chemical quantum.

Competing Interests

The authors have declared that no competing interests exist.

References

Arzaee, N. A., Noh, M. F. M., Ab Halim, A., Rahim, M. A. F. A., Ita, N. S. H. M., Mohamed, N. A., ... & Teridi, M. A. M. (2021). Cyclic voltammetry-A promising approach towards improving photoelectrochemical activity of hematite. Journal of Alloys and Compounds, 852, 156757. **https://doi.org/10.1016/j.jallcom.2020.156757**

Babić-Samardžija, K., & Hackerman, N. (2006). Iron corrosion inhibition with dihydrobis-and hydrotris-(1-pyrazolyl) borates. Anti-Corrosion Methods and Materials. **https://doi.org/10.1108/00035590610637438**

Blachowicz, T., & Ehrmann, A. (2020). Recent developments of solar cells from PbS colloidal quantum dots. Applied Sciences, 10(5), 1743. **https://doi.org/10.3390/app10051743**

Burns, R. M. (1936). The corrosion of metals—I. Mechanism of corrosion processes. Bell System Technical Journal, 15(1), 20-38. **https://doi.org/10.1002/j.1538-7305.1936.tb00717.x**

Chauhan, D. S., Quraishi, M. A., Ansari, K. R., & Saleh, T. A. (2020). Graphene and graphene oxide as new class of materials for corrosion control and protection: Present status and future scenario. Progress in

Organic Coatings, 147, 105741. https://doi.org/10.1016/j.porgcoat.2020.105741

Dubas, S. T., & Schlenoff, J. B. (2001). Swelling and smoothing of polyelectrolyte multilayers by salt. Langmuir, 17(25), 7725-7727. https://doi.org/10.1021/la0112099

Feng, X., Liu, Z., Qin, L., Kang, S. Z., & Li, X. (2020). Photocatalytic activity and the electron transport mechanism of titanium dioxide microsphere/porphyrin implanted with small size copper. Physical Chemistry Chemical Physics, 22(24), 13528-13535. https://doi.org/10.1039/D0CP01953D

Gan, J., He, J., Hoye, R. L., Mavlonov, A., Raziq, F., MacManus-Driscoll, J. L., ... & Qiao, L. (2019). α-CsPbI3 colloidal quantum dots: synthesis, photodynamics, and photovoltaic applications. ACS Energy Letters, 4(6), 1308-1320. https://doi.org/10.1021/acsenergylett.9b00634

Gao, J., Wang, X., Zhai, W., Liu, H., Zheng, G., Dai, K., ... & Shen, C. (2018). Ultrastretchable multilayered fiber with a hollow-monolith structure for high-performance strain sensor. ACS applied materials & interfaces, 10(40), 34592-34603. https://doi.org/10.1021/acsami.8b11527

Georgopoulou, A., & Clemens, F. (2020). Piezoresistive elastomer-based composite strain sensors and their applications. ACS Applied Electronic Materials, 2(7), 1826-1842. https://doi.org/10.1021/acsaelm.0c00278

Godínez, F. A., Mayén-Mondragón, R., Guzmán, J. E. V., Chávez, O., Gavaises, M., & Montoya, R. (2020). Bioinspired snapping-claw apparatus to study hydrodynamic cavitation effects on the corrosion of metallic samples. Review of Scientific Instruments, 91(6), 066101. https://doi.org/10.1063/5.0007069

Jones, D. (1992). Principles and prevention of corrosion. Macmillan Publishing Company(USA), 1992,, 568.

Joy, J., Cheriya, R. T., Nagarajan, K., Shaji, A., & Hariharan, M. (2013). Breakdown of Exciton Splitting through Electron Donor–Acceptor Interaction: A Caveat for the Application of Exciton Chirality Method in Macromolecules. The Journal of Physical Chemistry C, 117(35), 17927-17939. https://doi.org/10.1021/jp403431w

Khaled, K. F. (2008). Molecular simulation, quantum chemical calculations and electrochemical studies for inhibition of mild steel by triazoles. Electrochimica Acta, 53(9), 3484-3492. https://doi.org/10.1016/j.electacta.2007.12.030

Lahbib, H., Ben Hassen, S., Gerengi, H., Rizvi, M., & Ben Amor, Y. (2021). Corrosion inhibition performance of dwarf palm and Cynara cardunculus leaves extract for St37 steel in 15% H2SO4: a comparative study. Journal of Adhesion Science and Technology, 35(7), 691-722. https://doi.org/10.1080/01694243.2020.1819701

Lebrini, M., Bentiss, F., Vezin, H., & Lagrenée, M. (2006). The inhibition of mild steel corrosion in acidic solutions by 2, 5-bis (4-pyridyl)-1, 3, 4-thiadiazole: structure–activity correlation. Corrosion Science, 48(5), 1279-1291. https://doi.org/10.1016/j.corsci.2005.05.001

Lei, B., Xu, D., Wei, B., Xie, T., Xiao, C., Jin, W., & Xu, L. (2021). In situ synthesis of α-Fe2O3/Fe3O4 heterojunction photoanode via fast flame annealing for enhanced charge separation and water oxidation. ACS applied materials & interfaces, 13(3), 4785-4795. https://doi.org/10.1021/acsami.0c19927

Li, M., Zang, S., Wang, Y., Li, J., Ma, J., Zhang, X., & Liu, Y. (2021). Facile sputtering enables double-layered ZnO electron transport layer for PbS quantum dot solar cells. Solar Energy, 214, 599-605. https://doi.org/10.1016/j.solener.2020.11.042

Li, Y., Lu, X., Wu, K., Yang, L., Zhang, T., & Wang, F. (2020). Exploration the inhibition mechanism of sodium dodecyl sulfate on Mg alloy. Corrosion Science, 168, 108559. https://doi.org/10.1016/j.corsci.2020.108559

Liu, H., Wang, H., Qian, Y., Zhuang, J., Hu, L., Chen, Q., & Zhou, S. (2019). Nitrogen-doped graphene quantum dots as metal-free photocatalysts for near-infrared enhanced reduction of 4-nitrophenol. ACS Applied Nano Materials, 2(11), 7043-7050. https://doi.org/10.1021/acsanm.9b01549

Mehta, H., Kaur, G., Chaudhary, G. R., & Prabhakar, N. (2021). Assessment of bio-corrosion inhibition ability of Hafnium based cationic metallosurfactant on iron surface. Corrosion Science, 179, 109101. https://doi.org/10.1016/j.corsci.2020.109101

Messali, M., Larouj, M., Lgaz, H., Rezki, N., Al-Blewi, F. F., Aouad, M. R., ... & Chung, I. M. (2018). A new schiff base derivative as an effective corrosion inhibitor for mild steel in acidic media: Experimental and computer simulations studies. Journal of Molecular Structure, 1168, 39-48. https://doi.org/10.1016/j.molstruc.2018.05.018

Onyeachu, I. B., & Solomon, M. M. (2020). Benzotriazole derivative as an effective corrosion inhibitor for low carbon steel in 1 M HCl and 1 M HCl+ 3.5 wt% NaCl solutions. Journal of Molecular Liquids, 313, 113536. https://doi.org/10.1016/j.molliq.2020.113536

Tom, A. E., Thomas, A., & Ison, V. V. (2020). Novel post-synthesis purification strategies and the ligand exchange processes in simplifying the fabrication of PbS quantum dot solar cells. RSC Advances, 10(51), 30707-30715. https://doi.org/10.1039/D0RA05242F

Wang, M. C., Sheng, G. D., & Qiu, Y. P. (2015). A novel manganese-oxide/biochar composite for efficient removal of lead (II) from aqueous solutions. International Journal of Environmental Science and Technology, 12(5), 1719-1726. https://doi.org/10.1007/s13762-014-0538-7

Xing, M., Wei, Y., Wang, R., & Zhang, Z. (2021). Study on the performance of ZMO/PbS quantum dot

heterojunction solar cells. Solar Energy, 213, 53-58. **https://doi.org/10.1016/j.solener.2020.11.023**

Xiong, Y., Yang, L., Zhu, Y., Lai, Q., Li, P., Xiao, P., & Cao, G. (2021). Tuning Electronic Structure of 2D In2S3 via P Doping and Size Controlling Toward Efficient Photoelectrochemical Water Oxidation. Solar RRL, 5(1), 2000618. **https://doi.org/10.1002/solr.202000618**

Yang, F., Ke, Z., Li, Z., Patrick, M., Abboud, Z., Yamamoto, N., ... & Gu, J. (2020). Photo/Bio-Electrochemical Systems for Environmental Remediation and Energy Harvesting. ChemSusChem, 13(13), 3391-3403. **https://doi.org/10.1002/cssc.202000203**

Younis, S. A., Kwon, E. E., Qasim, M., Kim, K. H., Kim, T., Kukkar, D., ... & Ali, I. (2020). Metal-organic framework as a photocatalyst: Progress in modulation strategies and environmental/energy applications. Progress in Energy and Combustion Science, 81, 100870. **https://doi.org/10.1016/j.pecs.2020.100870**

Zhang, R., Li, S., Ying, C., Hu, Z., Lv, A., Hu, H., ... & Wong, C. P. (2020). Bioinspired design of flexible strain sensor with high performance based on gradient filler distributions. Composites Science and Technology, 200, 108319. **https://doi.org/10.1016/j.compscitech.2020.108319**

Zhu, H., Li, X., Lu, X., Chen, X., Li, J., Han, X., ... & Hu, Z. (2021). Intra-/inter-molecular synergistic inhibition effect of sulfonate surfactant and 2-benzothiazolethiol on carbon steel corrosion in 3.5% NaCl solution. Corrosion Science, 182, 109291. **https://doi.org/10.1016/j.corsci.2021.109291**